Flow instabilities in a graft anastomosis: A study of the instantaneous velocity fields
C J Bates, D M O'Doherty and D Williams

The online version of this article can be found at:
http://pih.sagepub.com/content/215/6/579

Published by:
$SAGE

http://www.sagepublications.com

On behalf of:

**Institution of
MECHANICAL
ENGINEERS**

Institution of Mechanical Engineers

Additional services and information for *Proceedings of the Institution of Mechanical Engineers, Part H: Journal of Engineering in*
Medicine **can be found at:**

Email Alerts: http://pih.sagepub.com/cgi/alerts

Subscriptions: http://pih.sagepub.com/subscriptions

Reprints: http://www.sagepub.com/journalsReprints.nav

Permissions: http://www.sagepub.com/journalsPermissions.nav

Citations: http://pih.sagepub.com/content/215/6/579.refs.html

>> Version of Record - Jun 1, 2001

What is This?

Flow instabilities in a graft anastomosis: a study of the instantaneous velocity fields

C J Bates, **D M O'Doherty*** and **D Williams**
Division of Mechanical Engineering and Energy Studies, Cardiff School of Engineering, Cardiff University, Wales, UK

Abstract: The major cause of arterial bypass graft failure is intimal hyperplasia. Fluctuating wall shear stresses in the graft, which are associated with disturbed flow, are believed to be important factors in the development and localization of intimal hyperplasia. This study, based upon water as the working fluid, has investigated the flow structure inside a 30° Y-junction with different fillet radii at the intersection between the graft and the host artery at various Reynolds numbers and distal outlet segment (DOS) to proximal outlet segment (POS) flow ratios. The structure of the flow has been investigated experimentally using particle image velocimetry (PIV). The two-dimensional instantaneous velocity fields confirm the existence of a very complex flow, especially in the toe and heel regions for the different fillet radii and clearly identify features such as sinks, sources, vortices and strong time dependency.

Keywords: anastomosis, flow fields, time dependency

NOTATION

d	pipe diameter (m)
PIV	particle image velocimetry
QVF	quick visible flow
Re	Reynolds number
t_i	time of first PIV image (s)
t_p	time interval between PIV images (s)
$\bar{u}$	mean velocity (m/s)
ν	kinematic viscosity (m²/s)

1 INTRODUCTION

A variety of theories have been proposed regarding the cause of atherosclerosis. Most experts, including physicians, believe that in addition to the complex biochemical processes, haemodynamic factors play an important role in atherogenesis. This is because most atherosclerotic lesions are found in the vicinity of bends and bifurcations of medium to large arteries. The influence of the local haemodynamics on the biological processes leading to the disease is not well understood. The flow patterns in these areas exhibit unique characteristics, which are usually characterized by flow recirculation, long particle residence times, abnormal values and variations of the wall shear stresses. It is obvious that these local disturbed flow patterns are related to the atherogenic process. Therefore, detailed studies of flow phenomena occurring at bends and bifurcations may contribute to a better understanding of the role of haemodynamic factors in the process of atherosclerosis.

Although arterial graft bypasses are generally end-to-side bifurcations, most studies have been focused on Y-shaped bifurcations. For example, the flow pattern around the carotid bifurcation has been studied by numerous people who correlated the intimal thickness with the wall shear stresses for pulsatile and non-pulsatile flows with both Newtonian and non-Newtonian fluids as well as investigating the effects of distensible walls [1–8].

For end-to-side branches, most research work has focused on experimental studies using such techniques as laser Doppler anemometry (LDA) [9–11], flow visualization and cinemicrographic techniques [12, 13], and dye-injection techniques [14]. Although these studies investigated the effects of both Newtonian and non-Newtonian fluids for different graft angles, they did not investigate the wall shear stresses. However, two research groups have, within the last 10 years, measured the spatial and temporal variations of wall shear stress and investigated the relationship between the intimal thickening and wall shear stresses as well as the effects of model compliance and fluid rheology on the results [15–19].

In addition to these experimental studies, various researchers have created numerical simulations of the graft in an attempt to provide a full quantitative picture of the flow field and estimates of the wall shear stresses, especially for complicated geometries under pulsatile flow conditions [20, 21]. They have considered two-dimensional representations of a fully three-dimensional problem and have estimated the wall shear stress distributions in 45° end-to-side anastomoses with both rigid and flexible walls under physiological flow conditions; estimations were for Newtonian and non-Newtonian fluids in both steady and unsteady flow conditions.

Fei et al. [22], have investigated the three-dimensional flow pattern and wall shear stress variation in a distal graft anastomoses with different branching angles. However, they assumed steady flow conditions and a graft to artery diameter ratio of 1 : 1. According to Lou and Yang [23], a steady flow simulation will cause substantial errors. This observation is strongly supported by the detailed measurements reported by Bates et al. [24]. Kleinstreuer et al. [25], studied the effect of many geometric factors on the local haemodynamics of a three-dimensional model. The geometric factors considered included the bifurcation angle, the wall curvatures, the graft to artery area ratio as well as the flowrates and their directions. Their studies showed that the single best indicator of non-uniform haemodynamics was the wall shear stress gradient. In particular they showed that with the base case junction (i.e. a graft to artery diameter ratio of 1 : 1, a bifurcation angle of 30° and relatively sharp corners) significant flow field improvements can be achieved by changing the geometry. The changes to the geometry that were suggested included increasing the flow area ratios, smaller but variable bifurcation angles and smooth junction curvatures whenever possible.

The current paper provides, for the first time, detailed particle image velocimetry (PIV) measurements of the flow field within a 50 mm diameter graft model. The measurements are taken under pulsatile flow conditions with a mean Reynolds number of 500–10 000, based on water as the working fluid. The results show the structure of the vortices, their time-dependent nature and subsequent transport. These results complement the detailed LDA measurements presented by Bates et al. [24] which confirmed the turbulent nature of the flow as seen in the reported velocity profiles, intermittent nature of the flow and power spectral density plots.

2 EXPERIMENTAL TECHNIQUES

Three idealized scaled models of an arterial bypass anastomosis were manufactured from 50 mm internal diameter QVF transparent glass. These were used to study the flow structure within a 30° Y-junction with a fillet radius of 5, 15 or 25 mm. A fully developed sinusoidal wave pulsatile flow at the three Reynolds numbers of 500, 2000 and 10 000 was pumped through the junction such that the flow ratio between the distal outlet segment (DOS) and the proximal outlet segment (POS) was 80 : 20, 60 : 40 or 40 : 60. The flow at the junction inlet was controlled such that the water was pumped at three specific Reynolds numbers of 500, 2000 and 10 000, where Reynolds number was defined as

$$Re = \frac{\bar{u}d}{\nu}$$

Full details of the flow facility have been presented previously in the literature [24]. The flow characteristics through the junction were then monitored non-intrusively using PIV techniques, which allow the measurements of the instantaneous two-dimensional velocity field.

2.1 The PIV system

The velocity of a fluid is measured throughout a region illuminated by a two-dimensional high-energy light sheet (Fig. 1). The source of this light sheet is, normally, a laser, since many lasers have a pulsed output with both controlled pulse duration and repetition rate. The seeding of any measured flow relies upon particles, which follow the flow; they should be near neutrally buoyant and scatter light efficiently. Particles are introduced to the flow and their motion is used to visualize and measure the kinematics of the local fluid. The inability of the particles to mimic the exact movements of the fluid leads to errors in the PIV technique.

For this study, a Dantec FlowMap PIV system was used. The system comprised a small portable pulsed laser for light-sheet illumination together with recording and processing equipment for analysis of the flow field. The laser used was a New Wave Research Mini YAG pulsed laser, which provided 50 mJ with laser pulses of 10 ms duration, on a green wavelength of 532 nm. The minimum interval between the laser pulses was 66.75 ms.
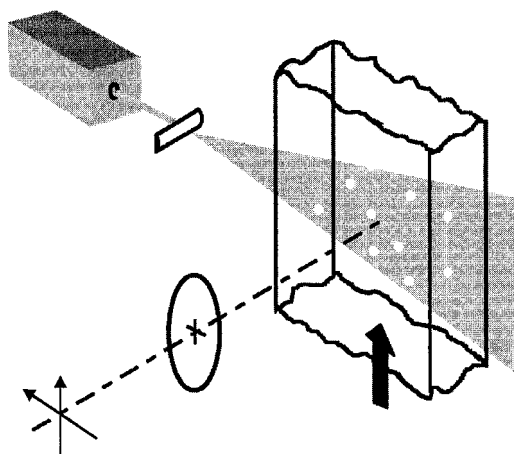

Fig. 1 Experimental arrangement for PIV measurements

Satisfactory illumination was achieved by seeding the flow with 15–20 μm diameter ground mica. The expected velocity error due to the inability of the seed particles to follow the fluid oscillation both within and outside any recirculation regions has previously been confirmed to be less than 0.5 per cent (Sierra-Espinosa [26]).

The motion of the particles is recorded using multiple exposure photographic methods. The PIV images are recorded using digital recording media, a charge-coupled device (CCD) camera. The CCD camera was positioned at 90° to the laser sheet (Fig. 1). This is necessary to avoid distortion of the image. One disadvantage is that the intensity of the light scattered by the particle has a local minimum at 90°.

In this instance the CCD camera was a DoubleImage 700 CCD camera which had a maximum frame rate of 30 Hz, with a Nikon zoom lens, 35–70 mm, f 3.3–4.5 and a chip resolution of 1024×1024 pixels. This resulted in a pixel dimension of 8.9×6.6 μm giving a pixel pitch of 11.6 μm in the horizontal direction and 13.6 μm in the vertical direction. The recorded images were digitized directly in the camera and transferred to the computer. The result of the recording was two images of the particle, one at t_i and the second at $t_i + t_p$, where t_p was set to 66.75 ms. The PIV images were analysed using the cross-correlation method, noting that the estimation of the fluid's velocity assumes that no acceleration of the seeding particle occurs during the flight from the first image capture position to the second image capture position. This means that the velocity magnitude and direction are constant. The cross-correlation method saves each image of the double picture one after the other in a frame. Each frame is then subdivided into small interrogation areas, ensuring that the flow within an interrogation area is essentially homogeneous. This means that the smallest spatial scales in the flow should not be less than the spatial resolution of the system. For this study, the interrogation area was set to 64×64 pixels that provided the optimal match between the spatial and dynamic ranges.

To apply the PIV technique to this graft geometry, a Perspex viewing box containing water was built to encase the 30° Y-junction completely. A similar box was designed by Sierra-Espinosa in 1997 [26]. The purpose of this box was to reduce light distortion caused by the change in the refraction index between the pipe's glass wall and the air by putting another fluid in contact with the pipe wall. The distortions reduce the quality of the light scattered by the particle, which reduces the quality of the measured data. Ideally this other fluid's index of refraction must match that of the glass, but with a refractive index of the liquid closer to that of the wall, the problem is significantly reduced; the design employed is shown in Fig. 2.

3 RESULTS

3.1 Velocity vectors

PIV measurements in the vertical plane were undertaken to investigate the flow structure inside the 30° Y-junction. The PIV measurements obtained were instantaneous near real-time whole velocity fields. The PIV data complement the conventionally acquired time-averaged single-point LDA results. The use of conventional LDA systems requires several hours in order to acquire enough data to show the complex flow structure inside the 30° Y-junction, whereas the PIV system could achieve this within minutes. However, in this study the dimensional resolution of the measurements with the PIV was not as high as that achieved with the LDA system. LDA does not provide an instantaneous picture of the details of the local flow separation, but rather an averaged flow field over an extended period.

The PIV velocity fields viewed by the optical arrangement were not large enough to span the whole length of the junction, therefore six different frame locations had to be taken and then joined together, manually. Fifty individual successive frames were taken, at various time intervals depending on the flow condition, at each of these six locations in order to detect any time-dependent
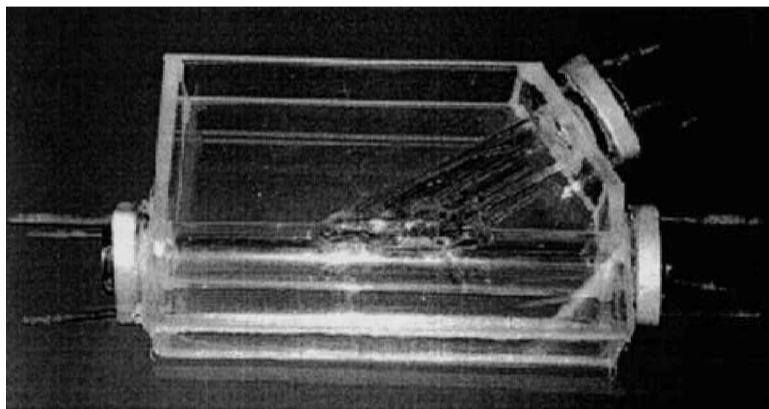

Fig. 2 Photo showing a 30° Y-junction encased inside the viewing box

characteristics of the flow (Fig. 3). This study was restricted to 50 frames per location because of the memory limitation of the computer. Each instantaneous vector plot contains details of the time-dependent nature of the flow. For all the figures presented, the bottom 10 mm, vertically, in the frames is not meaningful, this region was caused by the reflection of the laser from the glass wall of the pipe.

3.2 Instantaneous velocity fields—low Reynolds number

Figure 4 shows the instantaneous velocity over a section of the junction in the toe region; as identified in Fig. 3, at time t_i, the region extends from 50 to 130 mm from the DOS exit for the 25 mm fillet radius; Reynolds number was 500 and the DOS:POS ratio was 40:60. Even at this low Reynolds number the complexity of the flow is clearly evident. The inlet flow comprising the peak (long) velocity vectors, which reach 0.017 m/s, are shown

to impact against the floor of the junction, at distances greater than 100 mm. A swirling motion is set up, at the periphery, centred on the pipe centre-line. The flow then spirals along the wall and is effectively lost to the PIV system, which is focused on the vertical centre-line plane. In the toe region of the flow a point source, point S_1, is clearly evident, at 89 mm axially and 43 mm vertically. From the source the fluid is shown to enter the measurement plane and flow radially outwards, with peak velocities of 0.005 m/s, towards the upper wall of the toe, point A. From the source, some of the velocity vectors grow in strength as they become entrained and aligned into the strong inlet jet. Regions of negative flow are clearly evident in Fig. 4. Figure 5 shows the same region one time interval later $(t_i + t_p)$, the same salient source and entrainment features are present. However, the boxed region, B_2, in Fig. 5 shows different velocity vectors in comparison with box B_1 for the same region in Fig. 4. Instead of a zero axial component in B_1, a clear negative flow is present in B_2. For this low Reynolds
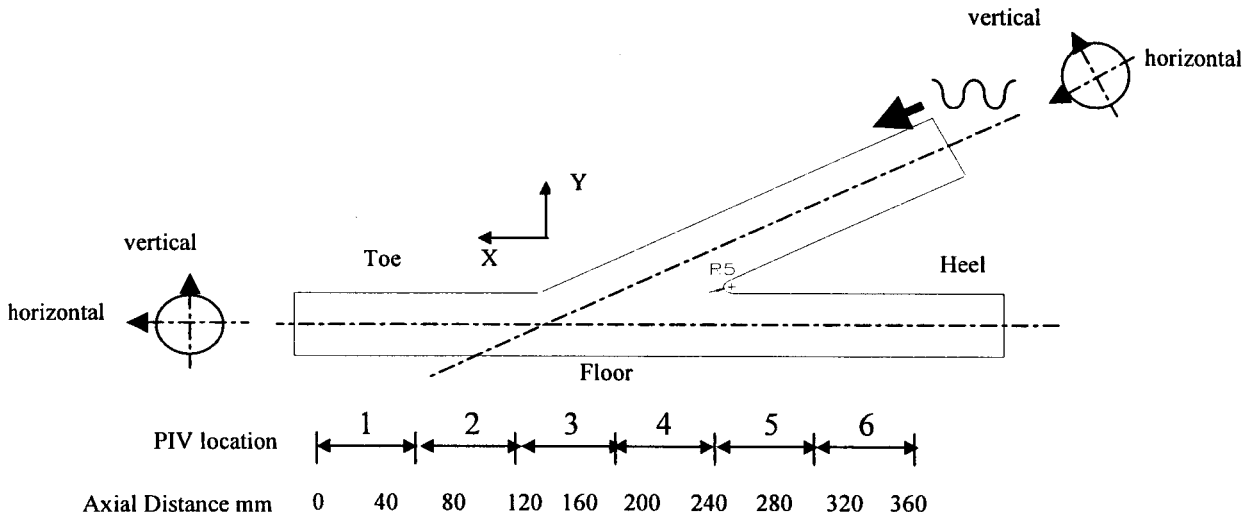
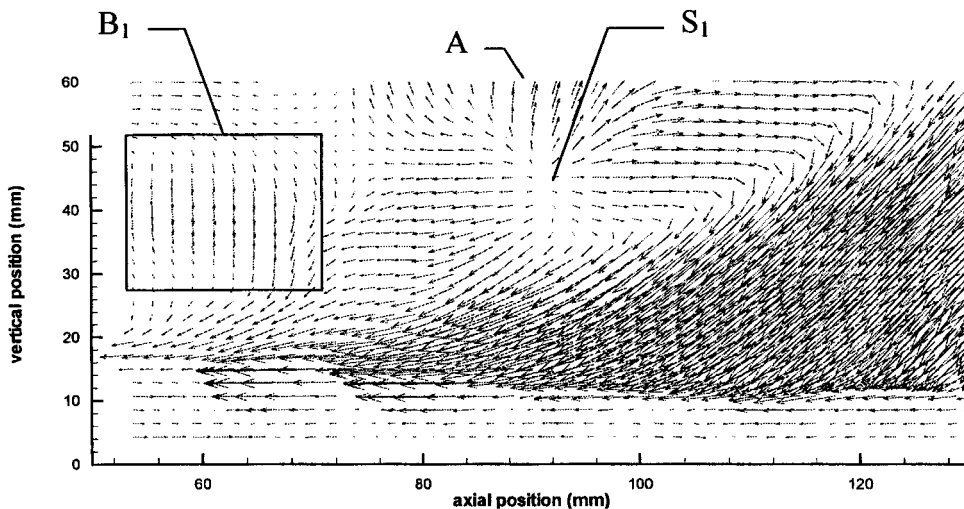

Fig. 3   Details of the coordinate system

Fig. 4   Flow field for 25 mm fillet radius, *Re* 500, DOS:POS 40:60 at time t_i
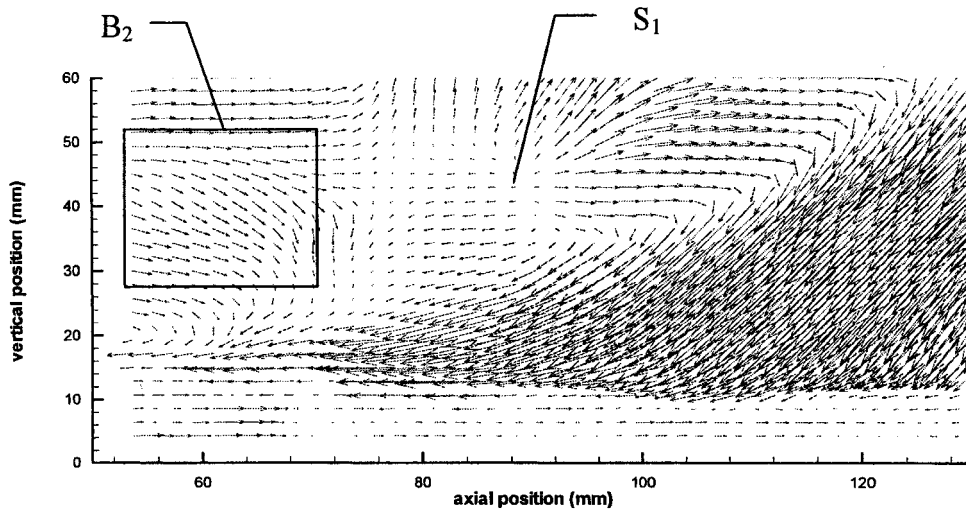
                H04900 © IMechE 2001

Fig. 5 Flow field for 25 mm fillet radius, *Re* 500, DOS : POS 40 : 60 at time $t_i + t_p$

number the flow in the toe region is reasonably stable, with strong entrainment, however, some time dependency or intermittency is observed in the recirculation region. At both the DOS and POS exits, the PIV measurements show that the vectors are aligned in the positive sense across the whole diameter.

3.3 Instantaneous velocity fields—high Reynolds number

The velocity vector plots in the vertical plane for the 5-mm-radius junction for a Reynolds number of 10 000 and a DOS : POS ratio of 80 : 20 are shown in Fig. 6. The figure covers the heel region location, which extends from 285 to 365 mm from the junction's distal outlet. Figure 6a provides details of the instantaneous velocity vectors observed on the centre-line plane, at time t_i, whereas Fig. 6b shows the same region at time $t_i + t_p$, where t_p is 66.75 ms. A large vortex, V_1, is evident in Fig. 6a, located 325 mm axially and 35 mm vertically.

Peak absolute velocities of 0.131 and 0.122 m/s are evident at points W and X for Fig. 6a and b, In Fig. 6b, vortex V_1 is still present but it has been transported downstream towards the POS exit. Comparison of Fig 6a and b confirms the presence of negative flow vectors adjacent to the heel of the junction.

Figure 7 shows the same region at $t_i + 5t_p$, the vortex shown in the previous figures has been transported out of the frame although a new vortex appears to be forming at 300 mm axially and 42 mm vertically (V_2 in Fig. 7). The negative flow region has been reduced in both size and intensity due to the presence of a large positive flow region which extends over the whole width of the frame, peak velocity being 0.16 m/s at point Y.

Figure 8 shows the same region at $t_i + 18t_p$, quite clearly now the positive and negative regions meet across an angled front. The negative flow dominates over the

boxed region B_3, while the strong positive flows reverse the negative flow's direction over the zone identified as B_4. A vortex V_3 is also being formed due to the shear layer between the positive and negative flow directions.

The frequency of the pulsatile flow (13.5 Hz) and the PIV's sampling rate (66.75 ms) are such that under ideal circumstances the flow cycle visualized should be repeated every 28 frames. Figure 9 shows the frame at $t_i + 28t_p$ which should be directly related to Fig. 6a. Comparison of these figures shows a weaker vortex, V_4, exists at the correct location in Fig. 9. However, the dominant velocity vectors (peak velocity of 0.115 m/s at Z), in the POS sense are located further downstream in Fig. 9 compared with Fig. 6a. In addition, the negative flow contribution is much weaker (size and strength) in Fig. 9. In general the PIV flow characteristics at this higher Reynolds number confirm that the flow is unsteady, time dependent and random. These are the very features that are used to define turbulence.

4 DISCUSSION

The instantaneous velocity fields obtained by the PIV system displayed the structure of the vortices and their time-dependent nature. The flow inside each of the three junctions was seen to adopt a variety of structures from one frame to another. The main vortices located under the toe and heel of the junction, for most flow conditions, were seen to enlarge and contract randomly and the vortices were then shed downstream, proximally.

The PIV data were not analysed in a similar manner to the LDA data previously discussed by Bates *et al.* [24] due to the relatively small number of frames recorded (50 frames). Many more frames would be required, with much smaller pixel spacing in order to provide accurate turbulence data from the PIV system.
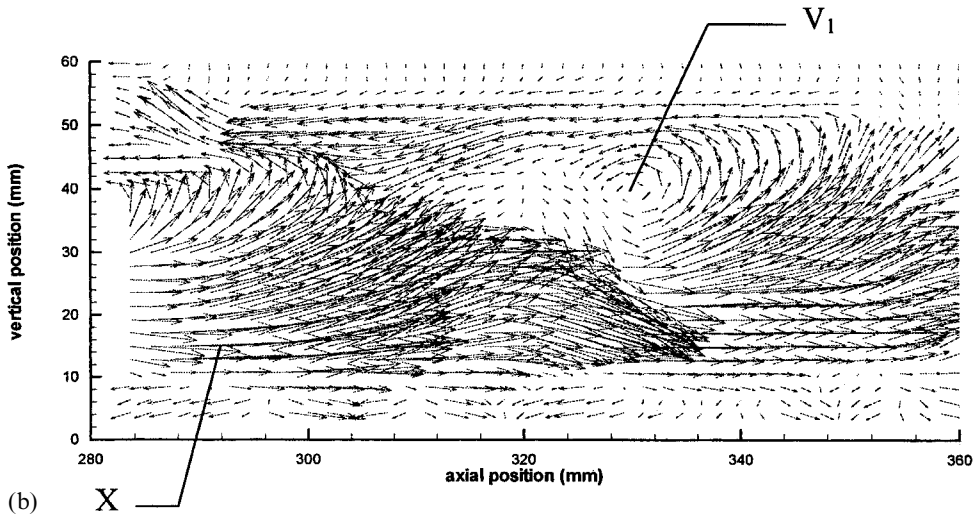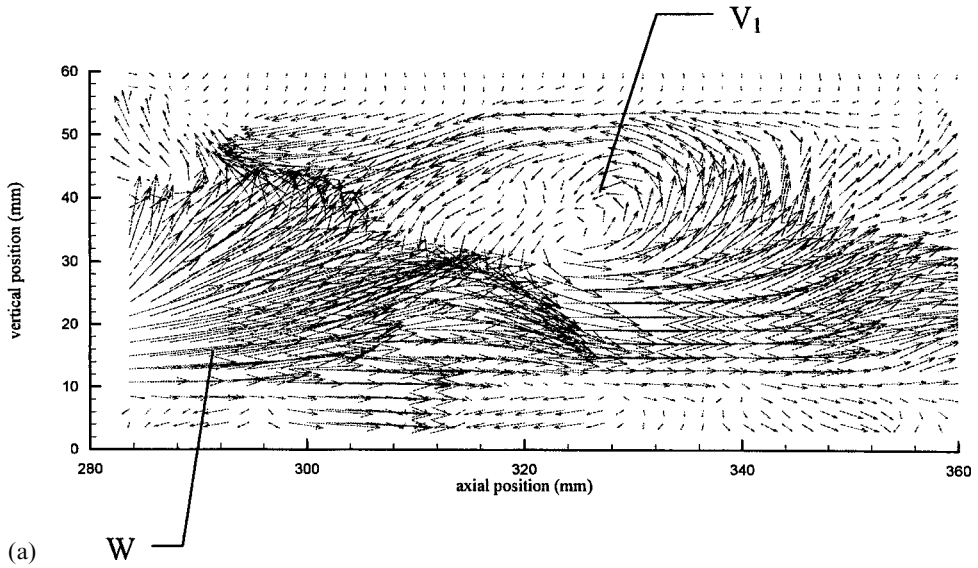
(a)

(b)

Fig. 6   Instantaneous velocity vectors: (a) time $= t_i$; (b) time $= t_i + t_p$
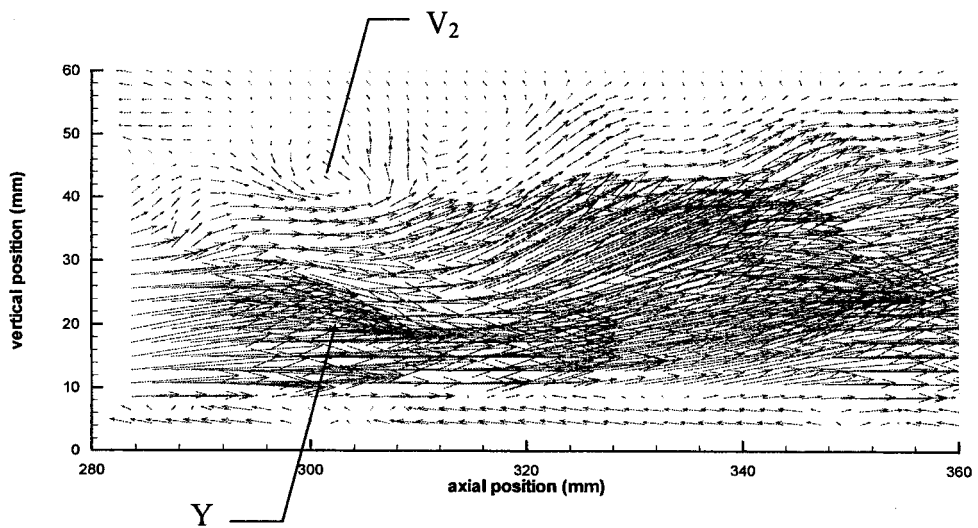

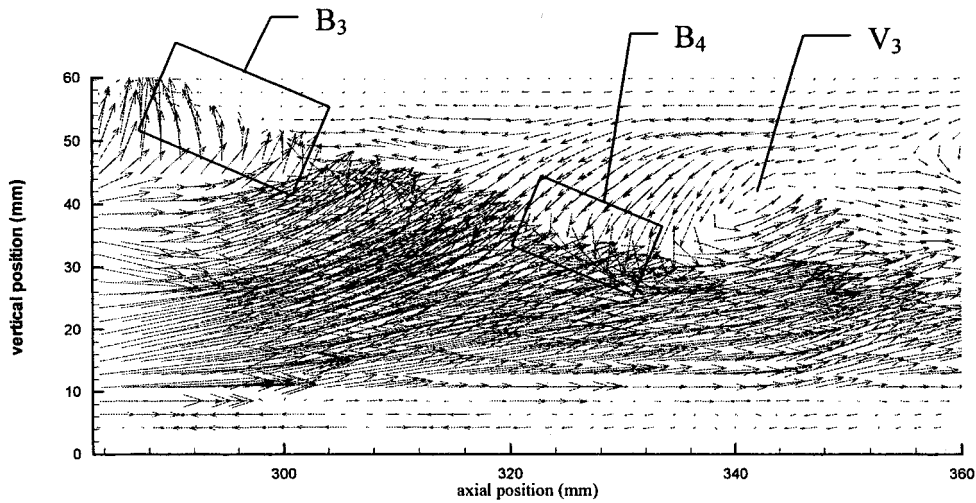**Fig. 7**   Instantaneous velocity vectors, time $= t_i + 5t_p$

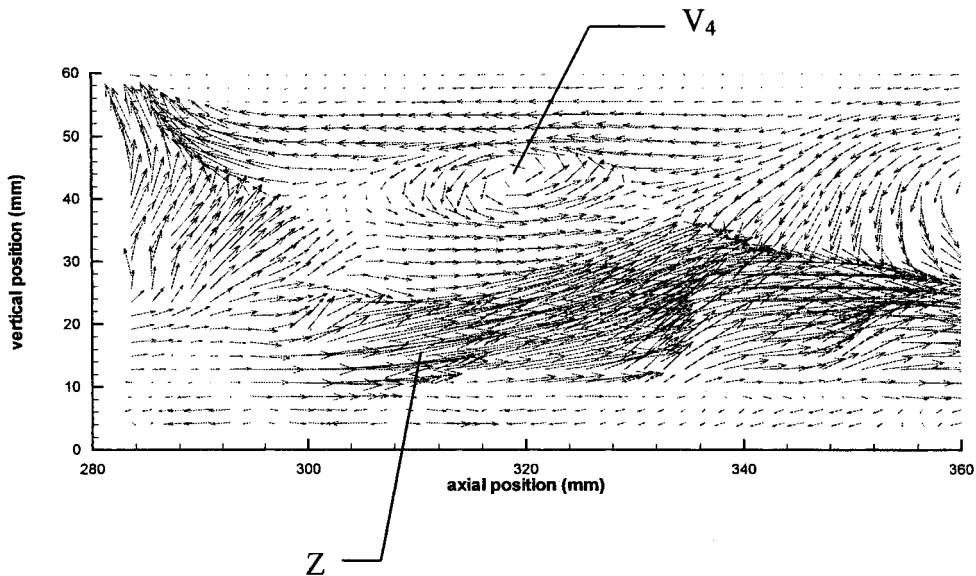**Fig. 8**   Instantaneous velocity vectors, time $= t_i + 18t_p$

Fig. 9   Instantaneous velocity vectors, time $= t_i + 28t_p$

The two sets of velocity data, the one-dimensional LDA data reported by Bates *et al.* [**24**] and the current two-dimensional PIV data, show close agreement with only marginal differences and essentially the same order of velocity magnitudes. The measurements, both the LDA and the PVI data, display all the essential flow characteristics in the junction, for all junction geometries and flow conditions. The location of the essential flow characteristics in both sets of data correlate closely with each other.

The histological data on intimal thickening in vascular grafts showed regions of intimal thickening at the heel, toe and floor of the graft as well as on the lateral walls near the suture lines [**27**, **28**]. Due to the large geometric and flow condition variability of vascular grafts, it was difficult to make a firm correlation between haemodynamic variables and intimal thickening. Measurement accuracy of the floor intimal thickening position was

important because the velocity of the flow changes drastically near the stagnation region on the floor of the junction. The velocity of the flow changes from near the maximum velocity to zero velocity over a short distance causing a region of very high shear stresses. The floor intimal thickening position, calculated from many anteriograms, appeared to be located in the stagnated flow region. It was observed that the flow separation point on the floor moved proximally and distally over a pulse. This movement would cause the wall shear stress on the floor to fluctuate drastically, which as discussed promotes the development of intimal hyperplasia.

The toe intimal thickening is attributed to the separation region located along the upper toe, observed when the proximal outlet flow was dominant, i.e. DOS:POS flow ratios of 60:40 and 40:60. When the DOS:POS flow ratio was 80:20, separation appeared at the lower toe caused by the inability of the distal flow to follow

the wall around the 30° corner and forcing the bulk flow towards the floor of the junction.

From the instantaneous PIV frames it was observed that the flow was time dependent (unsteady). The vortex located under the heel of the junction moves, proximally and distally, with the pulse as it was formed (driven by the inlet flow) then shed downstream, proximally. The movement of the vortex causes the shear stresses on the wall of the junction near the heel to oscillate. Oscillations in the wall shear stress are known to be a contributing factor to the development of intimal hyperplasia, which explains the region of hyperplasia located at the heel of a vascular graft.

The higher Reynolds numbers in this study have been included to demonstrate that the environment varies appreciably inside a graft when the body is exercising. The wall shear stresses and flow patterns inside the graft vary significantly when the body exercises, these conditions were believed to reduce the progression of intimal thickening in a vascular graft. Flow visualization performed by Giddens et al. [29], implemented exercise conditions to the end-to-side graft model used by White et al. [30]. Under exercise flow conditions, particles that had settled in regions of low wall shear stresses during resting flow conditions, low Reynolds numbers, were cleared in a few pulsatile cycles. The possible implication of this increased flow during exercise is that it minimizes regions of low wall shear stresses throughout the junction, which reduces the probability of the development of intimal hyperplasia.

This present study reinforces the majority of the discoveries of other researchers such as Loth [31]. The major discovery of this PIV study was to identify the importance of the impact that occurs against the floor, as the fluid flows through the junction, this mechanism has a significant influence on the DOS and POS turbulence structure. The location where the inlet flow impacted the junction floor was governed by the DOS : POS flow ratio and the mean Reynolds number.

5   CONCLUSION

This study has investigated the flow structure inside a 30° Y-junction (designed to represent an arterial bypass graft) with various fillet radii at the intersection between the graft and the host artery at various Reynolds numbers and DOS : POS flow ratios. The structure of the flow has been investigated experimentally. For analysis of pulsatile flow through a 30° Y-junction, the PIV system has provided a convenient economical means for the qualitative and quantitative study of the flow patterns. The two-dimensional PIV results compared well with the corresponding one-dimensional LDA results which confirms the validity of the current PIV results in both magnitude of velocity and the location of the flow structures, i.e. vortices.

The essential flow features in the junction, such as the stagnation point on the junction floor and the vortex under the heel, were identified from the measurements by means of the velocity data. It was observed that the positions of all the essential flow features inside the junction move distally and proximally over a pulse cycle. The movement of these structures causes the shear stress on the junction wall to fluctuate. It is known that low or fluctuating wall shear stresses lead to the formation of intimal thickening and eventually graft failure.

Following this research there was enough information available concerning the effect of various graft variables such as graft : host artery diameter ratios, graft angle, intersection fillet radius, DOS : POS flow ratio, etc., on the flow inside the graft to lead to the optimal graft design. This study has introduced evidence of the change in the character of the flow once it has impacted against the flow junction floor. The impact on the floor is believed to be a contributing factor to graft failure. To minimize the dissipation of energy from the pulse it is suggested that the method of introducing the inlet flow smoothly into the junction should be improved.

REFERENCES

1 Ku, D. N., Giddens, D. P., Zarins, C. K. and **Glagov, S.** Pulsatile flow and atherosclerosis in the human carotid bifurcation—positive correlation between plaque location and low oscillating shear stress. *Arteriosclerosis*, 1985, **5**(3), 293–302.

2 Ku, D. N. and **Giddens, D. P.** Laser Doppler anemometer measurements of pulsatile flow in a model carotid bifurcation. *J. Biomechanics*, 1987, **20**(4), 407–421.

3 Kleinstreuer, C., Nazemi, M. and **Archie, J. P.** Haemodynamics analyses of a stenosed carotid bifurcation and its plaque mitigating design. *J. Biomech. Engng*, 1991, **113**, 330–335.

4 Lou, Z. and **Yang, W. J.** A computer simulation of the blood flow at the aortic bifurcation with flexible walls. *J. Biomech. Engng*, 1993, **115**, 306–315.

5 Anayoitos, A. S., Jones, S. A., Giddens, A. P., Glagov, S. and **Zarins, C. K.** Shear stress at a compliant model of the human carotid bifurcation. *J. Biomech. Engng*, 1994, **116**, 98–106.

6 Kuban, B. D. and **Friedman, M. H.** The effect of pulsatile frequency on wall shear in a compliant cast of a human aortic bifurcation. *J. Biomech. Engng*, 1995, **117**, 219–223.

7 Perktold, K., Peter, R. and **Resch, M.** Pulsatile non-Newtonian blood flow simulation through a bifurcation with an aneurysm. *Biorheology*, 1990, **26**, 1011–1030.

8 Xu, X. Y., Collins, M. W. and **Jones, C. J. H.** Flow studies in canine artery bifurcations using a numerical simulation method. *J. Biomech. Engng*, 1992, **114**, 504–509.

9 Liepsch, D., Moravec, S., Rastogi, A. K. and **Vlachos, N. S.** Measurement and calculations of laminar flows in a ninety degree bifurcation. *J. Biomechanics*, 1982, **15**(7), 473–485.

10 Liepsch, D. and **Moravec, S.** Pulsatile flow of non-Newtonian fluid in distensible models of human arteries. *Biorheology*, 1984, **21**, 571–586.

11 Keynton, R. S., Rittgers, S. E. and **Shu, M. C.** The effect of angle and flow rate upon haemodynamics in distal vascular graft anastomoses: an *in vitro* model study. *J. Biomech. Engng*, 1991, **113**, 458–463.

12 Karino, T. and **Goldsmith, H. L.** Particles flow behaviour in models of branching vessels: effects of branching angle and diameter ratio on flow patterns. *Biorheology*, 1985, **22**, 87–104.

13 Karino, T., Motomiya, M. and **Goldsmith, H. L.** Flow patterns at the major T-junctions of the dog descending aorta. *J. Biomech. Engng*, 1990, **112**, 537–548.

14 Crawshaw, H. M., Quist, W. C., Serrallach, E., Valeri, R. and **LoGerfo, F. W.** Flow disturbance at the distal end to side anastomosis: effect of patency of the proximal outflow segment and angle of anastomosis. *Arch. Surg.*, 1980, **115**, 1280–1284.

15 Ojha, M. Spatial and temporal variations of wall shear within an end-to-side arterial anastomoses model. *J. Biomechanics*, 1993, **26**(12), 1377–1388.

16 Ojha, M., Cobbold, R. S. and **Johnston, K. W.** Haemodynamics of a side to end proximal arterial anastomosis. *J. Vascular Surgery*, 1993, **17**, 646–655.

17 Ojha, M. Wall shear stress temporal gradient and anastomic intimal hyperplasia. *Circulation Res.*, 1994, **74**, 1227–1231.

18 Friedman, M. H., Bargeron, C. B., Duncan, D. D., Hutchins, G. M. and **Mark, F. F.** Effects of arterial compliance and non-Newtonian rheology on correlations between intimal thickness and wall shear. *J. Biomech. Engng*, 1992, **114**, 317–320.

19 Friedman, M. H. Arteriosclerosis research using vascular flow models from 2-D branches of compliant replicas. *J. Biomech. Engng*, 1993, **115**, 595–601.

20 Steinman, D. A., Vinh, B., Ethier, C. R., Ojha, M., Cobbold, R. S. C. and **Johnston, K. W.** A numerical simulation of flow in a two-dimensional end-to-side anastomosis. *J. Biomech. Engng*, 1993, **115**, 112–118.

21 Steinman, D. A. and **Ethier, C. R.** The effect of wall distensibility on flow in a two-dimensional end-to-side anastomosis. *J. Biomech. Engng*, 1994, **116**, 294–301.

22 Fei, D. Y., Thomas, J. D. and **Rittgers, S. E.** The effect of angle and flow rate upon haemodynamics in distal vascular graft anastomoses: a numerical model study. *J. Biomech. Engng*, 1994, **116**, 331–336.

23 Lou, Z. and **Yang, W. J.** Biofluid dynamics at arterial bifurcations. *Biomed. Engng*, 1992, **19**(6), 455–493.

24 Bates, C. J., O'Doherty, D. M. and **Williams, D.** Experimental and computational modelling of flow through an arterial bypass graft. In *Cardiovascular Flow Modelling and Measurement with Application to Clinical Medicine* (Eds S. G. Sajjadi, G. B. Nash and M. W. Rampling), 1999 (Oxford University Press).

25 Kleinstreuer, C., Lei, M. and **Archie, J. P.** Flow input waveform effects on the temporal and spatial wall shear stress gradients in femoral graft–artery connector. *J. Biomech. Engng*, 1996, **118**, 346–354.

26 Sierra-Espinosa, F. Z. The turbulence structure of the flow in a 90° pipe junction: a comparison of numerical predictions to experimental laser Doppler and particle image velocimetry results. PhD thesis, University of Wales, Cardiff, 1997.

27 Sottiurai, V. S., Yao, J. S. T., Batson, R. C., Sue, S. L., Jones, R. and **Nakamura, Y. A.** Distal anastomotic intimal hyperplasia: histopathologic character and biogenesis. *Ann. Vascular Surgery*, 1989, **3**(1), 26–33.

28 Bassiouny, H. S., White, S., Glagov, S., Choi, E., Giddens, D. P. and **Zarins, C. K.** Anastomotic intimal hyperplasia: mechanical injury or flow induced. *J. Vascular Surgery*, 1992, **15**, 708–717.

29 Giddens, E. M., Giddens, D. P., White, S. S., Zarins, C. K., Bassiouny, H. S. and **Glagov, S.** Exercise flow conditions eliminate stasis at vascular graft anastomoses. In Proceedings of the 3rd Mid-Atlantic Conference on *Biofluid Mechanics*, 1990, pp. 225–267 (New York University Press, New York).

30 White, S. S., Zarins, C. K., Giddens, D. P., Bassiouny, H. S., Loth, F., Jones, S. A. and **Glagov, S.** Haemodynamic patterns in flow models of end to side vascular graft anastomoses: effect of pulsatility, flow division, Reynolds number and hood length. *J. Biomech. Engng*, 1993, **115**, 104–111.

31 Loth, F. Velocity and wall shear measurement inside a vascular graft model under steady and pulsatile flow conditions. PhD thesis, Georgia Institute of Technology, Georgia, 1993.